

Detection Recovery in Online Multi-Object Tracking with Sparse Graph Tracker

Jeongseok Hyun^{1*} Myunggu Kang² Dongyoon Wee² Dit-Yan Yeung¹
¹Hong Kong University of Science and Technology ²Clova AI, NAVER Corp.

Abstract

Joint object detection and online multi-object tracking (JDT) methods have been proposed recently to achieve one-shot tracking. Yet, existing works overlook the importance of detection itself and often result in missed detections when confronted by occlusions or motion blurs. The missed detections affect not only detection performance but also tracking performance due to inconsistent tracklets. Hence, we propose a new JDT model that recovers the missed detections while associating the detection candidates of consecutive frames by learning object-level spatio-temporal consistency through edge features in a Graph Neural Network (GNN). Our proposed model Sparse Graph Tracker (SGT) converts video data into a graph, where the nodes are top- K scored detection candidates, and the edges are relations between the nodes at different times, such as position difference and visual similarity. Two nodes are connected if they are close in either a Euclidean or feature space, generating a sparsely connected graph. Without motion prediction or Re-Identification (ReID), the association is performed by predicting an edge score representing the probability that two connected nodes refer to the same object. Under the online setting, our SGT achieves state-of-the-art (SOTA) on the MOT17/20 Detection and MOT16/20 benchmarks in terms of AP and MOTA, respectively. Especially, SGT surpasses the previous SOTA on the crowded dataset MOT20 where partial occlusion cases are dominant, showing the effectiveness of detection recovery against partial occlusion. Code will be released at <https://github.com/HYUNJS/SGT>.

1. Introduction

Tracking-by-detection (TBD) is a dominant framework for multi-object tracking (MOT) that detects objects and associates them across frames in a video. Initially, two-stage models are proposed based on two or three separate models for detection and association (*i.e.*, tracking) [5, 6, 36, 44, 49, 52, 56, 65], but the performance is sub-optimal, and the inference speed is slow. To address these issues, end-to-end

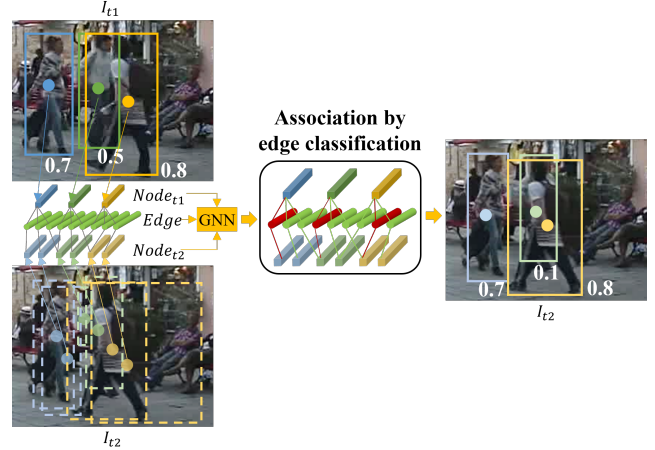


Figure 1. Three pedestrians are detected with their detection scores above the detection threshold (e.g., 0.5) at t_1 , but the green box is missed at t_2 due to its low confidence score (0.1) caused by partial occlusion. Our model associates top- K scored detections candidates (e.g., 6), instead of the detections above the threshold. GNN outputs edge features which are higher-order relational features considering neighboring edges. These edge features are effective in associating the objects correctly as shown in the red lines which are the positive edges. Then, the missed detection (the green box) is recovered in an association step.

(E2E) jointly trainable detection and tracking (JDT) methods are proposed in [2, 9, 30, 37, 42, 47, 60, 63]. However, all these methods only use the positive detections which confidence score is above a detection threshold value for association. Partial occlusion as shown by the green box in Figure 1 results in the missed detection that the confidence score of true detection is below the detection threshold. Such missed detections consequently lead to inconsistent trajectory of tracklets due to frequent disconnections. Accordingly, finding the detection threshold that achieves the best trade-off between false positives and true positives is crucial.

Online MOT methods are required to output tracklets at every timestep; thus, missed detections should be recovered in an online manner as well. Existing works utilize temporal cues based on previous frames to reduce missed detections. Chained-Tracker [37] and CenterTrack [63] use extra convolution layers with input of two consecutive frames.

*The work was partially done during an intern at Clova AI.

GSDT [46], CorrTracker [45], and TransTrack [43] propose using GNN [32], correlation layer [15], and transformer [66] to enhance the features for detection and tracking, respectively. These methods are effective in reducing missed detection, but they still have an issue that low-confident true detections are excluded from association, leading to missing tracklets.

In an association stage, existing online MOT works utilize pairwise relational features between two detections, such as the similarity of appearance features [26, 30, 45–47, 54, 60], the center distance [63], and the Intersection over Union (IoU) score [43]. These features reflect only the relations between two objects and are not discriminative enough for accurate matching in a crowded scene. Extra tracking components such as a motion predictor (*e.g.*, Kalman filter [4], or a learnable offset head [63]) are commonly employed to improve online MOT performance. On the contrary, we jointly use all these pairwise relational features to initialize edge features and update them to higher-order (multi-hop) relational features by aggregating the features of neighboring nodes and edges through GNN. Without a motion predictor, the higher-order relational features are strong enough to match tracklets with the current frame’s (I_{t2}) top- K scored detections including low-scored detections. Originally missed detection due to low confidence score is recovered in association by edge classification as shown in Figure 1.

The main contributions of this work are as follows:

1. Sparse Graph Tracker (SGT) is a new MOT model that recovers missed detections in an online manner while matching detection candidates of consecutive two frames.
2. SGT is a graph-based online MOT model that performs both short-term and long-term association in a single step without relying on a motion predictor (*e.g.*, Kalman filter [4]).
3. SGT achieves MOTA of 76.7/76.3/72.8% while running at 23.0/23.0/19.9 FPS using a single V100 GPU in the MOT16/17/20 benchmarks, respectively. SGT shows a large improvement in the MOT20 benchmark which is vulnerable to missed detections due to crowded scenes.

2. Related works

2.1. JDT Methods

Joint object detection and multi-object tracking (JDT) became a principal methodology for MOT due to its simplicity and performance. Recently proposed JDT methods fall into two categories: (1) jointly training of the detection and ReID tasks in a single image, and (2) predicting the motion between consecutive frames.

JDT by ReID. Siamese Track-RCNN [42], RetinaTrack

[30], and JDE [47] extend object detectors Faster-RCNN [39], RetinaNet [28], and YOLOv3 [38], respectively, to JDT models by appending a ReID branch to the detector. FairMOT [60] improves this method by applying an anchor-free detector, CenterNet [64].

However, CStrack [26] points out that the objectives of detection and ReID are conflicting, and proposes a cross-correlation network that learns task-specific features. Recently, RelationTrack [54] developed this line of works by learning more discriminative ReID features by considering the relation between objects in an image. Similarly, GSDT [46] improves the features by spatio-temporal relational modeling through GNN. CorrTracker [45], which is the current SOTA model, fuses the correlation in spatial and temporal dimensions to the image features at multiple pyramid levels.

JDT by motion prediction. D&T [17] and CenterTrack [63] introduce object motion prediction to MOT model. While D&T uses correlation between feature maps of two consecutive frames, CenterTrack adds the feature maps and an object heatmap of the previous frame. Chained-Tracker [37] concatenates feature maps of consecutive frames and predicts paired boxes in two frames. TraDeS [50] predicts the offset of objects between two consecutive frames based on a cost volume which is computed by a similarity of ReID features of the frames. TransTrack [43] is a transformer-based model that propagates previous frame’s tracklets to the coordinates in current frame and matches with current frame’s detections by IoU score.

Comparison. Our SGT is also a JDT model based on CenterNet [64]. Compared with others using pairwise relations (*e.g.*, IoU or cosine similarity of ReID features), SGT exploits edge features, which are higher-order relational features generated through GNN, to solve tracking as an edge classification as shown in Figure 1.

2.2. Graph-based Multi-object Tracking

A graph is an effective way to represent relational information, and GNN learns higher-order relational information through a message passing process that propagates and aggregates neighboring features. STRN [52] is an online MOT method with a spatio-temporal relation network that consists of a spatial relation module and a temporal relation module. TNT [44] builds a graph using each short tracklet as a vertex and predicts the connectivity score between tracklets so that fragmented tracklets are connected. MPNTrack [6] adopts a message passing network [18] with time-aware node update module to solve MOT problem by exploiting both node and edge features from a batch of frames. LPCMOT [11] generates and scores tracklet proposals based on a set of frames and detections using a Graph Convolution Network (GCN) [22]. These models are either not JDT or not online methods.

GSDT [46] is the first work that applies a GNN in an online JDT method; however, a graph does not have edge features and the GNN is limited to only enhancing the node features reflecting spatio-temporal relations. In contrast, our SGT uses edge features for tracking with top- K detections and recovers the missed detections which confidence score is lower than the threshold.

2.3. Online Detection Recovery

ByteTrack [59] and OMC [27] are concurrent works sharing our motivation and performing an online detection recovery. In ByteTrack [59], the unmatched tracklets are matched with low-scored detections, which score is between the original detection threshold (τ_D) and a new introduced threshold ($\tau_{D_{low}}$), using IoU. OMC [27] uses cross-correlation between ReID features of previous tracklets and feature map of current frame to recover missed detections. Both works conduct detection recovery after or before association using pairwise relational features, but SGT integrates it in an association step exploiting edge features.

3. Sparse Graph Tracker

3.1. Overall Architecture

Figure 2 shows the architecture of SGT. While various image backbones and object detectors can be flexibly adopted, we experiment based on CenterNet [64] with a variant of the DLA-34 backbone [55] which is used in our baseline model, FairMOT [60]. Following [60], we modify CenterNet such that the box size predictor outputs left, right, top, and bottom sizes (s_l, s_r, s_t, s_b) from a center point of an object instead of its width and height. CenterNet is a point-based object detector that predicts objects at every pixel of a feature map. The score predictor outputs a heatmap which is denoted as $B_{score} \in \mathbb{R}^{H_h \times H_w \times 1}$, where H_h and H_w are height and width of the feature map. The output from the box size predictor is denoted as $B_{size} \in \mathbb{R}^{H_h \times H_w \times 4}$. The box offset predictor adjusts the center coordinates of objects using $B_{off} \in \mathbb{R}^{H_h \times H_w \times 2}$. At frame T , CenterNet finally outputs detections $D_T = (S_T, B_T)$, where $S_T \in \mathbb{R}^{H \times H \times 1}$ is the detection score (B_{score}) and $B_T \in \mathbb{R}^{H_h \times H_w \times 4}$ composed of the top-left and bottom-right coordinates of the boxes.

Sparse Graph Builder takes top- K scored detection candidates from each frame (I_{t1} and I_{t2}) and sets them as the nodes of a graph (N_{t1} and N_{t2}). In the inference phase, the previous timestep's N_{t2} will be the current timestep's N_{t1} . We sparsely connect N_{t1} and N_{t2} if they are close in either a Euclidean or feature space. Specifically, $n_{t1}^i \in N_{t1}$ is connected to N_{t2} with three criteria: 1) small distance between their center coordinates; 2) high cosine similarity between their features; 3) high IoU score. For each criterion, the given number of N_{t2} (e.g., 10) are selected to be connected

to n_{t1}^i without duplicates. The connections are bidirectional so that both N_{t1} and N_{t2} update their features. The visual features of the detection candidates and the relational features between them are used as the features of nodes (V) and edges (E), respectively.

To include detection candidates, we can introduce an extra low threshold value, τ_{low} , as an alternative to using top- K scored detection candidates. Although it can also achieve good performance as shown in Appendix, such detection threshold value is sensitive to the detector's score distribution. As a result, using τ_{low} requires careful calibration for different datasets. In contrast, top- K method is robust to such issues as it is not affected by the score distribution. Since K is the maximum number of objects that the model can detect, we set K to be sufficiently larger than the maximum number of people in the dataset (e.g., 100 in MOT16/17; 300 in MOT20). In Table 7, we experimentally show the robustness of K values.

Some tracklets fail to connect for a duration when they are invisible due to full occlusion. These missing tracklets are cached for a certain period (max_{age}) and used in long-term association. Existing MOT works [5, 45, 47, 50, 60] usually apply the motion predictor (e.g., Kalman filter [4]) to the missing tracklets, and then match with the new detections. In SGT, they are appended to N_{t1} and association can be performed in a graph without the motion predictor. Also, we introduce min_{age} which is the minimum length of the missing tracklets to be cached. When $min_{age} = 10$, the missing tracklets which were successfully matched for at least 10 frames are included in the graph.

Graph Neural Network updates the features of nodes (V) and edges (E) in the graph through a message passing process, as shown in Figure 3, that propagates the features to the neighboring nodes and edges and then aggregates those features. By iterating this process, V now contain features of both the neighboring nodes and edges and E indirectly aggregates the features of other edges which are connected to the same node. Further iteration allows the edges to have higher-order (multi-hop) edge features. Initial edge features represent the pairwise relation of two detection candidates; however, updated edge features represent the higher-order relation of neighboring detection candidates. More details can be found in Section 3.2.

Edge Classifier is a FC layer that predicts the edge score (ES) from the updated edge features. The edge score is the probability that the connected detection candidates at $t1$ and $t2$ refer to the same object. Since n_{t1}^i is connected to many nodes at $t2$, we use the Hungarian algorithm [23] for optimal matching based on the edge score matrix. As a result, n_{t1}^i has only one edge score which is optimally assigned. Then, the edge threshold (τ_E) is used for deciding a positive or negative edge. The yellow box shown in Figure 2 is the recovered detection that n_{t2}^3 is negative due to its

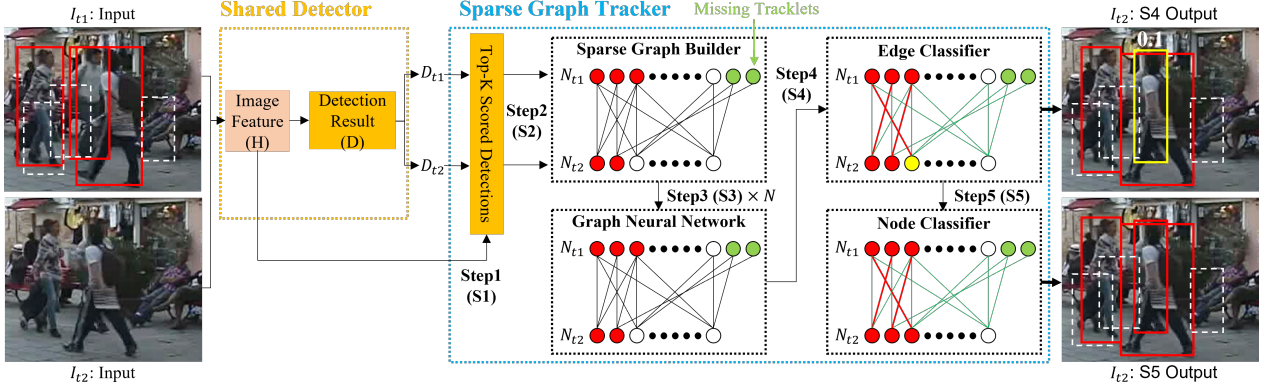


Figure 2. **Schematic of SGT.** (S1) Top- K scored detections and their features are extracted from I_{t1} and I_{t2} . The red boxes are positive detections which score above the detection threshold (τ_D) while the white boxes are top- K scored detections but below τ_D . (S2) A sparse graph is built, where a node, $n_T^i \in N_T$ ($i \in [1, K]$), is a detection candidate of frame $T = \{t1, t2\}$ and an edge ($e_{i,j}$) is a connection between n_{t1}^i and n_{t2}^j . The red nodes are positive detections. The green nodes are the tracklets that are missed until $t1$ and are appended to N_{t1} . (S3) GNN updates the features of nodes and edges to become higher-order by aggregating neighboring features. (S4) The edge score of the red line (a positive edge) is above the edge threshold (τ_E) while the green line represents a negative edge. The yellow node (n_{t2}^3) is an example of detection recovery. It was previously negative detection due to its low score, but it becomes a positive detection with the help of a positive edge. (S5) The recovered detection (n_{t2}^3) in S4 is verified by the node score. If the node score is below the node threshold (τ_N), it is regarded as a false positive and is filtered out. Otherwise, the node is recovered and hence can be successfully detected which is shown by the yellow node becoming red.

low detection score, but its connected node, n_{t1}^1 , and edge ($e_{1,3}$) are positive.

Node Classifier is a FC layer that prevents incorrect detection recovery by predicting the node score (NS) from the updated node features. If the recovered detection’s node score is below the node threshold (τ_N), we decide not to recover it, thus the node stays negative. Otherwise, we confirm recovery of the missed detection and the node becomes positive as shown by n_{t2}^3 in Figure 2.

3.2. Graph Construction and Update

Designing the node and edge features is crucial for graphs. Here, we use a FC layer, layer normalization [1] and ReLU activation function as a basic FC block.

Initial node features. Contrary to the graph-based MOT works using ReID features of detected objects [6, 48, 52], SGT exploits the image backbone’s visual features (H) which are shared for the detection task and jointly trained.

Initial edge features. We denote an edge feature as $e_{i,j}^l$, where i and j are the starting and ending node indices respectively, and l indicates iteration. Inspired by MPN-Track [6], SGT initializes high-dimensional edge features as Figure 1.

$$e_{i,j}^0 = f_{enc} \left(\left[x_i - x_j, y_i - y_j, \log\left(\frac{w_i}{w_j}\right), \log\left(\frac{h_i}{h_j}\right), IoU_{i,j}, Sim_{i,j} \right] \right), \quad (1)$$

where $[\cdot]$ is a concat operator, x and y are the center coordinates, h and w are the height and width of a bounding box, and f_{enc} refers to two FC blocks. As the initialized

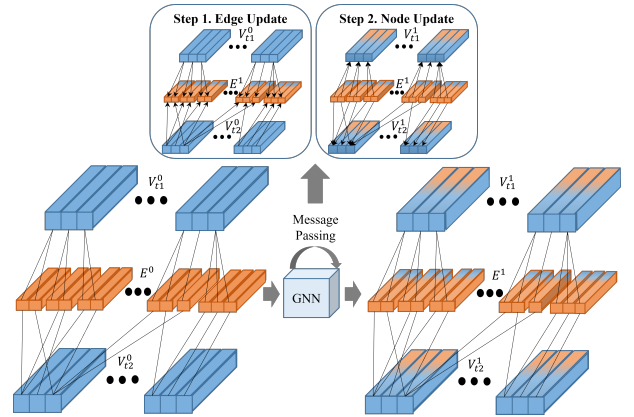


Figure 3. In GNN, the message passing process updates node and edge features in two steps. Firstly, initial edge features (E^0) are updated to E^1 containing the features of connected two nodes (V_{t1}^0 and V_{t2}^0). Secondly, initial node features (V^0) are updated to V^1 containing the features of connected nodes (V^0) and edges (E^1) which are already updated in the first step. For simplicity, we omit the bidirectional connection and show only few edges.

edge features are direction-aware, two edges connecting the same nodes but reversely will have different features considering different relations (e.g., $t1 \rightarrow t2$ and $t2 \rightarrow t1$). V_{t1} and V_{t2} are updated on two different MLPs with these different edge features. After updating in GNN, these bidirectional edge features are averaged to predict a single edge score.

Initial graph, shown in the left of Figure 3, is denoted by $G^0 = \{V^0, E^0\}$, where $E^0 = \{e_{i,j}^0 | 1 \leq i, j \leq 2K + |V_{miss}|\}$ is a set of initial edge features and $V^0 = V_{t1}^0 \cup V_{t2}^0 \cup V_{miss}^0$ is a set of initial node features at $t1$, $t2$, and missing tracklets.

Update in node and edge features. Figure 3 describes two steps to update the features of nodes and edges during the message passing process in GNN. The initial edge features $e_{i,j}^0$, shown in the left side of the graph, are pairwise relational features considering only the two connected nodes at $t1$ and $t2$ (direction $i \rightarrow j$).

In Step 1 of Figure 3, the edge features are updated as Eq. 2.

$$e_{i,j}^l = f_e([v_i^{l-1}, v_j^{l-1}, e_{i,j}^0, e_{i,j}^{l-1}]), \quad (2)$$

where f_e refers to two FC blocks, l is the number of iterations ($l \in [1, N_{iter}]$), v_i is the features of node i , and v_i^{l-1} indicates the node features of the previous iteration. Therefore, the current state of the two connected nodes, initial and current edge features are concatenated and passed to f_e to update edge features as $e_{i,j}^l$. Initial edge features ($e_{i,j}^0$) are concatenated every iteration to prevent the over-smoothing issue in GNN [34]. Although we use the shared MLPs (f_e) for the edges of two different directions, the edge features of the opposite direction may not be the same since their edge features are encoded in a direction-aware manner.

In Step 2 of Figure 3, node j aggregates the features of the connected nodes and edges as Eq. 3.

$$v_j^l = f_{v_{out}}\left(\frac{1}{|E_{:,j}^l|} \sum_i f_{v_{enc}}([v_i^{l-1}, e_{i,j}^l])\right), \quad (3)$$

where $f_{v_{out}}$ is an FC block, $|E_{:,j}^l|$ is the number of edges connected to the node j , $f_{v_{enc}}$ refers to two FC blocks, $e_{i,j}^l$ is the updated edge features in Step 1 (Eq. 2) and v_i^{l-1} is the features of starting node. We suppose the index of N_{t2} is from 1 to K and N_{t1} is from $K+1$ to $2K + |V_{miss}|$. When $i > j$, $e_{i,j}$ is the edge features with direction of $t1 \rightarrow t2$. Thus, message passing is from $t1$ to $t2$ and V_{t2} are updated. As our edge features are direction-aware, we use different $f_{v_{enc}}$ for message passing $t1 \rightarrow t2$ and $t2 \rightarrow t1$.

3.3. Training and Inference Strategies

SGT is trained by the sum of the detection loss (\mathcal{L}_D) and the association loss (\mathcal{L}_A).

Detection loss. Since we adopt CenterNet [64] as a detector, we follow [64] to compute the detection loss which is the weighted sum of losses from three heads as Eq. 4.

$$\mathcal{L}_D = \mathcal{L}_{score} + w_{size}\mathcal{L}_{size} + w_{off}\mathcal{L}_{off} \quad (4)$$

The size head outputs B_{size} composed of (s_l, s_r, s_t, s_b) . The offset head outputs B_{off} which is the quantization error of the center coordinates caused by the stride of feature map (e.g., 4). For each ground-truth (GT) object $\hat{b}^i =$

$(\hat{x}_l^i, \hat{y}_l^i, \hat{x}_r^i, \hat{y}_b^i)$, GT size $\hat{b}_{size}^i = (\hat{s}_l^i, \hat{s}_r^i, \hat{s}_t^i, \hat{s}_b^i)$ is computed by the difference between center coordinates $(\hat{c}_x^i, \hat{c}_y^i) = (\frac{\hat{x}_l^i + \hat{x}_r^i}{2}, \frac{\hat{y}_l^i + \hat{y}_b^i}{2})$ and \hat{b}^i . Each GT size \hat{b}_{size}^i is assigned to the prediction $b_{size}^{xy} \in B_{size}$, where $(x, y) = (\lfloor \frac{\hat{c}_x^i}{4} \rfloor, \lfloor \frac{\hat{c}_y^i}{4} \rfloor)$. Each GT offset $(\hat{o}_x, \hat{o}_y) = (\frac{\hat{c}_x^i}{4} - \lfloor \frac{\hat{c}_x^i}{4} \rfloor, \frac{\hat{c}_y^i}{4} - \lfloor \frac{\hat{c}_y^i}{4} \rfloor)$ is assigned to the prediction b_{off}^{xy} . Then, l_1 loss is used to compute \mathcal{L}_{size} and \mathcal{L}_{off} . For training the score head, GT heatmap $M^{xy} \in \mathbb{R}^{H_h \times H_w \times 1}$ is generated by the Gaussian kernel as Eq. 5.

$$M^{xy} = \sum_{i=1}^{N_D} \exp\left(-\frac{(x - \lfloor \frac{\hat{c}_x^i}{4} \rfloor)^2 + (y - \lfloor \frac{\hat{c}_y^i}{4} \rfloor)^2}{2\sigma_d^2}\right), \quad (5)$$

where N_D is the number of GT object and σ_d is computed by width and height of each object [24]. \mathcal{L}_{score} is computed as the pixel-wise logistic regression with the penalty-reduced focal loss [28].

Association loss. Our association loss is the weighted sum of the edge and node classification losses as Eq. 6.

$$\mathcal{L}_A = w_{edge}\mathcal{L}_{edge} + w_{node}\mathcal{L}_{node} \quad (6)$$

In SGT, the edge and node classifiers output the edge and node scores (ES and NS), respectively. \mathcal{L}_{edge} and \mathcal{L}_{node} are computed on these scores with the focal loss [28]. Since it is difficult to assign GT labels to the edges connecting the background patches, we exclude them in \mathcal{L}_{edge} as Eq. 7.

$$\mathcal{L}_{edge} = \frac{1}{N_{E+}} \sum_{e_{i,j} \in E} \begin{cases} \text{FL}(ES_{i,j}, ey_{i,j}), & \text{if } ny_i = 1 \text{ or } ny_j = 1; \\ 0 & \text{otherwise,} \end{cases} \quad (7)$$

where N_{E+} is the number of GT edges which at least one of the endpoints is positive, E is a set of edges in G , FL is the focal loss, edge in direction of $t1 \rightarrow t2$, $ey_{i,j}$ is the GT label of edge connecting the nodes n_i and n_j , and ny_i is the GT label of n_i . We compute \mathcal{L}_{node} only on the node scores at $t2$ as Eq. 8.

$$\mathcal{L}_{node} = \frac{1}{N_{N_{t2}^+}} \sum_{n_j \in N_{t2}} \text{FL}(NS_j, ny_j), \quad (8)$$

where $N_{N_{t2}^+}$ is the number of GT positive nodes at $t2$. We output zero when $N_{E+} = 0$ or $N_{N_{t2}^+} = 0$.

Node and edge label assignment is an essential step for computing the losses. MPNTrack [6] and other existing works [45, 47, 60] use GT boxes to train matching branch. Instead of training with GT boxes, we introduce using pseudo labels, which are prediction boxes, to train edge and node classifiers of SGT. Similar to one-to-one matching adopted in DETR [8], Hungarian algorithm [23] optimally matches the GT boxes and the prediction boxes based on their IoU score matrix; the matched GT object IDs are assigned to the prediction boxes. To prevent the misallocation

of GT ID, the assigned IDs are filtered out if IoU of their matching is lower than the threshold (*e.g.*, 0.5). This step is repeated for N_{t1} and N_{t2} to assign (ny_i and ny_j). Finally, the GT edge label ($ey_{i,j}$) is assigned to the edges by matching the IDs of nodes. An edge is labeled as 1 if the two connected nodes have the same GT ID, and 0 otherwise.

Adaptive Feature Smoothing is our proposed inference technique to deal with recovered detections. Recent online MOT models update appearance features of tracklets in an exponential moving average manner as introduced in JDE [47] following $emb_{t2}^{trk} = \alpha \times emb_{t1}^{trk} + (1 - \alpha) \times emb_{t2}^{det}$. This method updates the appearance features of tracklets adding the current detection features with the fixed weight, α . However, low-scored recovered objects have unreliable appearance features since they may suffer from the occlusion or blur. Therefore, we use adaptive weight computed by the object scores (S_T) as Eq. 9.

$$emb_{t2}^{trk} = emb_{t1}^{trk} \times \frac{S_{t1}}{S_{t1} + S_{t2}} + emb_{t2}^{det} \times \frac{S_{t2}}{S_{t1} + S_{t2}} \quad (9)$$

4. Experiments

4.1. Datasets and Implementation Details

Datasets. We train and evaluate on the datasets of the MOT16/17/20 Challenge [13,31]. Due to a small size of the MOT Challenge training dataset, JDE [47] introduces training with additional pedestrian detection and ReID datasets: ETH [16], CityPerson [57], CalTech [14], CUHK-SYSU [51] and PRW [62]. FairMOT [60] further introduces CrowdHuman [41], which is a pedestrian detection dataset. Recent SOTA models report high performance using these additional datasets. We also use CrowdHuman [41] as an additional training dataset. Since CrowdHuman does not have ID data and is a still image, we assign a unique ID to every bounding box and randomly warp an image to generate a pair of I_{t1} and I_{t2} .

Implementation details. SGT’s detector is initialized with the official CenterNet’s weight [64] pretrained on the COCO object detection dataset [29]. Our input image size is 1088×608 following and the output feature map size ($H_w \times H_h$) is 272×152 . We randomly sample two images in the interval of [1, 30] from MOT datasets. Following FairMOT [60], random flip, warping and color jittering are selected as data augmentation. The same augmentation is applied to a pair of images. We use Adam optimizer [21] with a batch size of 12 and initial learning rate (lr) of $2e^{-4}$ which drops to $2e^{-5}$. There are 60 training epochs and lr is dropped at 50. For training, we use 1 for w_{off} , 0.1 for w_{size} , w_{edge} , and 10 for w_{node} . For inference, we use 0.5, 0.4 and 0.4 as τ_D , τ_E and τ_N , respectively. These values are chosen empirically. We will release code for details.

Table 1. Detection evaluation on the MOT17/20Det Benchmark. The best result for each metric is bolded.

Benchmark	Method	AP↑	Recall↑	Precision↑	F1↑
MOT 17Det	FRCNN [39]	0.72	77.3	89.8	83.1
	GSDT [46]	0.89	90.7	87.8	89.2
	YTLAB [7]	0.89	91.3	86.2	88.7
	SGT (ours)	0.90	93.1	92.5	92.8
MOT 20Det	ViPeD20 [10]	0.80	86.5	68.1	76.2
	GSDT [46]	0.81	88.6	90.6	89.6
	SGT (ours)	0.90	91.6	92.6	92.1

4.2. MOT Challenge Evaluation Results

We submit SGT to the MOT16/17/20 Challenge and compare it with the recent SOTA online MOT models as shown in Table 1 and 2.

Evaluation metrics. We use the standard evaluation metrics for 2D MOT [3]: Multi-Object Tracking Accuracy (MOTA), ID F1 Score (IDF1), False Negative (FN), False Positive (FP), Identity Switch (IDS) [25]. While MOTA is computed by FP, FN and IDS to emphasize the detection performance, IDF1 [40] is a metric focused on the pure tracking performance. Also, mostly tracked targets (MT) and mostly lost targets (ML) represent the ratio of GT trajectories covered by a track hypothesis for at least 80% of their respective life span, and at most 20% of their respective life span, respectively. For MOT17/20 Detection Challenge, we use precision, recall, F1, and AP [29] which is the average precision taken over a set of reference recall values ([0:0.1:1]) with IoU threshold 0.5.

Evaluation results of MOT17/20 Detection. We evaluate the object detection performance on the MOT17/20Det Challenge and the results are shown in Table 1. For both MOT17/20Det, SGT achieves SOTA performance in every metric and outperforms GSDT [46] which is also based on CenterNet [64] and GNN. Especially, SGT’s high precision shows that it recovers missed detections effectively with few false positives. Node classifier’s filtering stage contributes to this result as shown in Table 3.

Evaluation results of MOT16/17. As shown in Table 2, in terms of MOTA, SGT achieves the highest and the second rank in MOT16/17, respectively, with the best trade-off between FP and FN. SGT also ranks the highest MT on both MOT16/17, and the lowest and the second lowest ML in MOT16/17, respectively. These results indicate that SGT generates stable and long-lasting tracklets, proving that SGT effectively recovers missed detections in association. Among the CenterNet-based models [35,45,46,50,54,58,60,63], CenterTrack [63], TraDeS [50], GSDT [46] and CorrTracker [45] use more than one frame to exploit the spatio-temporal cues. Although CorrTracker [45] shows marginally higher MOTA than SGT by 0.2% in MOT17, CorrTracker [45] exploits longer temporal cues with five previous frames, compared with ours using

Table 2. Evaluation results of ours and recent SOTA online JDT models under the “private detector” protocol on the MOT16/17/20 benchmarks. Note that the methods using tracklet interpolation in the post-processing step are excluded to strictly satisfy “online setting”. The values not provided by the paper are filled up with “-”. For each metric, the best is bolded and the second best is underlined.

Method	MOTA↑	IDF1↑	MT↑	ML↓	FP↓	FN↓	IDS↓
MOT16 [31]							
QDTrack [35]	69.8	67.1	41.6	19.8	9861	44050	1097
TraDes [50]	70.1	64.7	37.3	20.0	8091	45210	1144
CSTrack [26]	70.7	71.8	38.2	17.8	10286	41974	1071
KDMOT [58]	74.3	74.7	40.4	17.6	-	-	797
GSDT [46]	74.5	68.1	41.2	17.3	<u>8913</u>	36428	1229
FairMOT [60]	74.9	72.8	44.7	15.9	-	-	1074
RelationTrack [54]	75.6	75.8	43.1	21.5	9786	34214	448
OMC [27]	76.4	74.1	46.1	<u>13.3</u>	10821	31044	-
CorrTracker [45]	<u>76.6</u>	<u>74.3</u>	<u>47.8</u>	<u>13.3</u>	10860	<u>30756</u>	<u>979</u>
SGT (ours)	76.7	73.1	49.1	10.7	10689	30428	1420
MOT17 [31]							
CenterTrack [63]	67.8	64.7	34.6	24.6	18489	160332	3039
QDTrack [35]	68.7	66.3	40.6	21.9	26598	146643	3378
TraDes [50]	69.1	63.9	36.4	21.5	<u>20892</u>	150060	3555
CSTrack [26]	70.6	71.6	37.5	18.7	-	-	3465
TransCenter [53]	73.2	62.2	40.8	18.5	23112	123738	4614
GSDT [46]	73.2	66.5	41.7	17.5	26397	120666	3891
KDMOT [58]	73.4	73.8	41.4	16.7	-	-	3303
FairMOT [60]	73.7	72.3	43.2	17.3	27507	117477	3303
RelationTrack [54]	73.8	74.7	41.7	23.2	27999	118623	1374
TransTrack [43]	74.5	63.9	46.8	11.3	28323	112137	3663
OMC [27]	<u>76.3</u>	<u>73.8</u>	44.7	13.6	28894	<u>101022</u>	-
SGT (ours)	<u>76.3</u>	72.4	47.9	<u>11.7</u>	25983	102984	4578
CorrTracker [45]	76.5	73.6	<u>47.6</u>	12.7	29808	99510	3369
MOT20 [13]							
TransCenter [53]	58.3	46.8	35.7	18.6	35959	174893	4947
FairMOT [60]	61.8	67.3	68.8	7.6	103440	88901	5243
TransTrack [43]	64.5	59.2	49.1	13.6	28566	151377	3565
CorrTracker [45]	65.2	69.1	<u>66.4</u>	<u>8.9</u>	79429	<u>95855</u>	5183
GSDT [46]	67.1	67.5	53.1	13.2	31913	135409	<u>3131</u>
RelationTrack [54]	67.2	<u>70.5</u>	62.2	<u>8.9</u>	61134	104597	4243
SOTMOT [61]	68.6	71.4	64.9	9.7	57064	101154	4209
OMC [27]	<u>70.7</u>	67.8	56.6	13.3	22689	125039	-
SGT (ours)	72.8	<u>70.5</u>	64.3	12.8	<u>25165</u>	112897	2649

only one previous frame. TransTrack [43] and TransCenter [53] also exploit the spatio-temporal cues by aggregating the features in consecutive two frames as same as ours, but through a deformable transformer [66]. SGT achieves higher MOTA than both of them. In MOT17, OMC [27], which is also using online detection recovery mechanism, and CorrTracker [45] show lower FN than SGT; still, the decrease in FP of SGT exceeds the gap of FN by far, resulting a better trade-off between FP and FN.

One limitation of SGT is high IDS caused by lack of discriminative appearance features due to the absence of a ReID network, compared with others [26, 27, 45, 50, 54, 54, 60]. Also, in MOT17, occlusion is sometimes caused by non-human objects, such as vehicles, which are not included in top- K detections for relational modeling. Extension of SGT with a ReID network and open-world object detection [20] is a promising future work, but this paper fo-

cuses on showing the effectiveness of the proposed graph tracker performing detection recovery in an online manner.

Evaluation results of MOT20. MOT20 is a challenging dataset with severely crowded scenes. Specifically, on each frame, while MOT17 has 30 people, MOT20 has 170 people on average. The most crowded scenes of MOT20 have more than 200 people. Such crowded situation causes frequent partial occlusion between people, and existing methods suffer from missed detections with less confident detection output. Our proposed detection recovery method leads SGT to being robust on such crowded scenes so that SGT achieves SOTA in MOTA with a large gap as shown in Table 2. SGT surpasses CorrTracker [45], which MOTA is the highest in MOT17, by 7.6%. OMC [27] ranks the second in terms of MOTA, but SGT achieves better trade-off between FN and FP, and higher MOTA and IDF1 by 2.1% and 2.7%, respectively. This is attributed to the difference of features used for detection recovery; OMC [27] uses appearance feature similarity, which is pairwise relational features, while SGT uses edge features updated by GNN, which is higher-order relational features. We show the importance of higher-order features in Table 8.

Apart from MOTA, SGT achieves high IDF1 and low IDS in MOT20. In MOT20, IDS of SGT is the lowest, whereas it is higher than other methods in MOT16/17. Since the detection models are more vulnerable to the missed detections in the crowded scene, existing methods [45, 54, 60] use lower detection threshold; however, this leads to significantly high FP, and high IDS and low IDF1, consequently. In Appendix, we also analyze the ratio of recovered detections by each sequence in MOT20 and show that the sequences with high ratio of recovered detections achieve large improvement.

Running time. We measure the running time in terms of frames-per-second (FPS) using a single V100 GPU; SGT runs at 23.0/23.0/19.9 FPS on MOT16/17/20, respectively. For fair comparison, we select the methods reporting FPS measured on the same GPU. In MOT17, CorrTracker [45] and TransTrack [43] run at 14.8 and 10.0 FPS, respectively. In MOT20, CorrTracker [45] runs 8.5 FPS. SGT records much faster than them in both MOT17/20 because SGT performs relational modeling in the object-level sparsely compared with CorrTracker [45] and TransTrack [43] densely relational model features in the pixel-level.

Although FairMOT [60], SOTMOT [61], and OMC [27] all measure FPS using a single RTX 2080Ti GPU rather than V100 GPU, we can compare their decrease in FPS between MOT17 and MOT20. When the number of objects increases (MOT17 \rightarrow MOT20), their FPSs are dropped by half; specifically, 25.9 \rightarrow 13.2, 16.0 \rightarrow 8.5, and 13.2 \rightarrow 6.7 in the order of FairMOT [60], SOTMOT [61], and OMC [27]. However, SGT shows robustness of FPS (23.0 \rightarrow 19.9) since SGT does not use Kalman Filter [4]

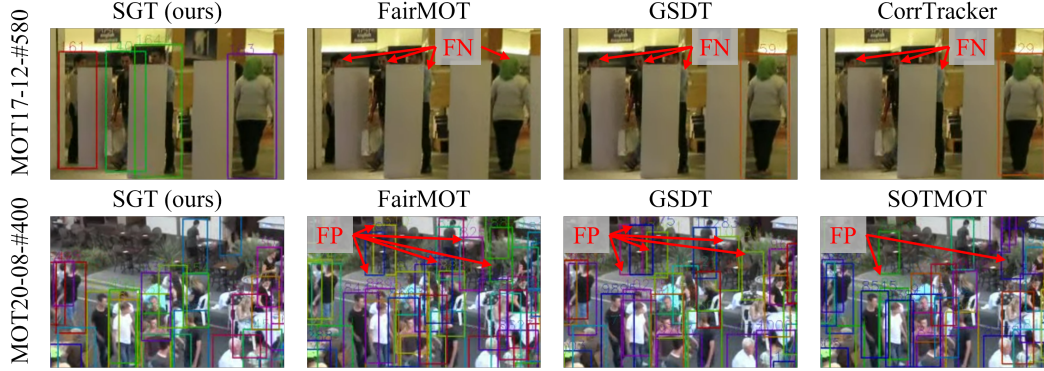


Figure 4. Qualitative comparison against CenterNet [64] based online JDT models [45, 46, 60, 61] in MOT17/20 Test which videos are available in MOT Challenge website. In MOT17, ours detects occluded people who are missed in the existing methods [45, 46, 60] based on the proposed detection recovery in association approach. In MOT20, ours does not have FP shown in the existing methods [46, 60, 61].

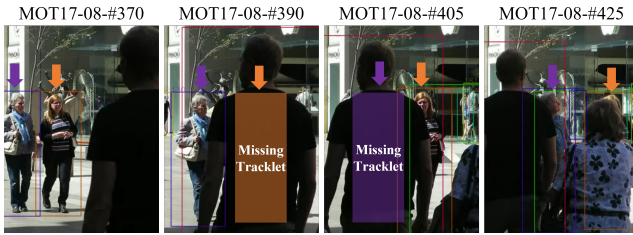


Figure 5. When the pointed people are fully occluded, the tracklets are missed in frame 390 and 405. SGT can perform long-term association without Kalman filter [4].

which running time increases proportional to the number of objects.

Visualization results. Figure 4 shows a qualitative comparison of SGT and other methods [45, 46, 60, 61]. In MOT17, partially occluded people are missed by FairMOT [60], GSDT [46], and CorrTracker [45], but SGT detects all of them. In MOT20, FairMOT [60], GSDT [46], and SOTMOT [61] all show FP detections on the chairs due to their low detection threshold; however, SGT does not have such FP without missed detections. Although SGT is robust against partial occlusion, detection recovery is failed and the tracklets are missed when the objects are fully occluded as shown in Figure 5.

4.3. Ablation Experiments

We conduct an ablation study to validate the effectiveness of each proposed module. We train FairMOT [60] and SGT on the first half of the MOT17 training dataset and evaluate it on the rest. Refer to Appendix for more details and results using different backbones.

Detection recovery. Table 3 shows the results of experiments comparing our GNN-based detection recovery architecture with another detection recovery method. BYTE [59]

Table 3. Ablation study of the detection recovery (DR) based on CenterNet [64]. DR-GNN denotes DR by the edge features. NC denotes filtering out recovered detections using the node classifier. BG denotes that top- K scored detections of I_{t1} are used as N_{t1} . Only detections above τ_D are used for measuring AP_{τ_D} , but recovered ones are included for τ_D .

Model	$AP_{\tau_D} \uparrow$	$AP (\Delta) \uparrow$	MOTA \uparrow	IDF1 \uparrow	FP \downarrow	FN \downarrow	IDS \downarrow
FairMOT [60]	71.6	71.6 (+0.0)	67.6	70.6	2346	14825	320
FairMOT [60] + BYTE [59]	71.6	73.4 (+1.8)	68.0	71.7	3306	13643	352
DR-GNN	73.6	77.2(+3.6)	70.3	72.8	3872	11521	671
DR-GNN + NC	73.6	76.4(+2.8)	70.6	70.8	2693	12323	870
DR-GNN + NC + BG (=SGT)	73.6	76.4(+2.8)	70.7	71.7	2724	12346	746

has an extra step associating unmatched tracklets with low-scored detections using IoU score, leading to the marginal improvement in overall but degradation in FP. Instead of performing detection recovery at a later stage, SGT matches tracklets with top- K detections including low-scored detections in a single step. Edge features, which are higher-order relational features yielded from iterations of GNN, better represent object-level spatio-temporal consistency than pairwise relational features, such as IoU; thus, using edge features for matching in SGT significantly decreases FN and increases AP attributed to recovered detections. To solve high FP issue, we add Step5 as shown in Figure 2 to filter out false positive recovered detections by node classification. As a result, better trade-off between FN and FP with lower FN can be achieved and consequently, MOTA is improved. In our final model, not only top- K scored detections of the $t2$ are used as nodes (N_{t2}) in a graph, but those of the $t1$ are also included in N_{t1} so that features of the background patches in the previous frame ($t1$) can be propagated to N_{t2} through the GNN iterations. This contributes to better IDF1 and IDS.

Long-term association. As shown in Table 4, introducing long-term association into SGT with max_{age} of one second increases IDF1 by 10.8%. We use min_{age} of ten frames

Table 4. Ablation study of the long-term association in SGT.

max_{age}	min_{age}	MOTA \uparrow	IDF1 \uparrow	FP \downarrow	FN \downarrow	IDS \downarrow
0 sec	0 frame	70.1	60.7	2495	12696	961
1 sec	0 frame	70.5	71.5	2987	12151	818
1 sec	1 frame	70.7	71.8	2916	12148	774
1 sec	5 frame	70.7	71.7	2803	12261	745
1 sec	10 frame	70.7	71.7	2724	12346	746

Table 5. Ablation study of training techniques. “J” and “P” denote joint training and pseudo labeling, respectively.

J	P	MOTA \uparrow	IDF1 \uparrow	FP \downarrow	FN \downarrow	IDS \downarrow
\times	\times	29.6	51.6	25490	10188	2396
\checkmark	\times	26.6	54.2	27885	9990	1776
\times	\checkmark	68.7	68.9	3395	12535	964
\checkmark	\checkmark	70.7	71.7	2724	12346	746

Table 6. Ablation study of feature smoothing in SGT. Note that we train SGT on CrowdHuman and MOT17 datasets, and evaluate on MOT17 Test server with different methods.

Weight	MOTA \uparrow	IDF1 \uparrow	MT \uparrow	ML \downarrow	FP \downarrow	FN \downarrow	IDS \downarrow
N/A	76.2	71.3	47.5	11.8	25998	103386	4797
fixed	76.3	71.7	47.6	11.8	26070	103215	4713
adaptive	76.3	72.4	47.9	11.7	25983	102984	4578

Table 7. FPS, memory and time consumption for training, and MOT17 validation performance with different K values.

K (Inference)	K (Train)	FPS \uparrow	MOTA \uparrow	IDF1 \uparrow	Memory	Train time
50	100	23.8	70.9	72.1	13.5 GB	3 hr
100	100	23.7	70.7	71.7	13.5 GB	3 hr
300	100	22.3	70.8	71.7	13.5 GB	3 hr
500	100	20.1	70.8	71.2	13.5 GB	3 hr
300	300	20.9	71.0	73.8	14.4 GB	3.5 hr
500	500	18.1	70.7	71.7	15.6 GB	4.5 hr

so that only the stable tracklets are cached and false positive recovery cases are avoided as much as possible. Figure 5 shows that SGT can match the missing tracklets without Kalman filter [4].

Training strategy. Table 5 shows training SGT with pseudo labeling is an important technique to reduce FP significantly. Using top- K detections as pseudo labels can generate edge labels of not only object-object pairs but also object-background pairs. Training with object-background pairs as extra negative examples helps SGT not to false positively match. Jointly training detection and tracking branches can further improve performance.

Adaptive feature smoothing. Naively update features with a fixed weight marginally improves IDF1 and IDS as shown in Table 6. In contrast, our proposed adaptive feature smoothing increases IDF1 and reduces IDS by a larger gap, proving its strength in SGT.

Robustness K value. We validate the robustness of K in SGT by training with different K values (e.g., 100, 300, 500) and inference with unseen K values (e.g., 50, 300, 500) using the model trained with $K = 100$. As shown in Table 7, consistent tracking performance is observed across different K values for training and unseen K values. Memory and time consumption for training and running time are

Table 8. Ablation study of the number of message passing iterations in GNN.

N_{iter}	MOTA \uparrow	IDF1 \uparrow	FP \downarrow	FN \downarrow	IDS \downarrow
0	66.2	69.0	2773	14775	731
1	69.6	69.3	2866	12675	895
2	68.2	69.8	2762	13646	792
3	70.7	71.7	2724	12346	746
4	70.8	71.9	2971	12027	805

also robust to increasing K .

Higher-order edge features. According to Table 8, the number of FN and IDS decreases as GNN iterates. This trend proves that the higher-order relational features are more effective in learning spatio-temporal consistency than the pairwise relational features ($N_{iter} = 0$). The performance saturates when $N_{iter} = 4$; thus, we decide to use $N_{iter} = 3$ which achieves the lowest FP and IDS.

5. Conclusion

Partial occlusion in a video leads to low-confident detection outputs, and the existing online JDT models suffer from missed detections since they only use the detections which confidence score is higher than the threshold. This paper presents SGT, a new approach of online JDT that can recover missed detections while associating top- K detections. With our proposed graph-based tracker, SGT effectively captures an object-level spatio-temporal consistency in video data by exploiting higher-order relational features of objects and background patches across time. This paper also proposes pseudo labeling and adaptive feature smoothing as training and inference techniques, respectively. The effectiveness of our proposed detection recovery is shown by SOTA performance in the MOT16/20 and MOT17/20 Detection benchmarks. In particular, SGT surpasses the current SOTA significantly in the MOT20 benchmark which is vulnerable to missed detections due to crowded scenes. SGT successfully performs detection recovery in the case of partial occlusion; still, detection recovery under full occlusion is yet to be solved. Possible future works are exploiting longer temporal cues and modeling the spatio-temporal relations of non-human objects (e.g., cars or traffic sign object) which can occlude humans. We hope SGT will serve as a new online MOT method which is robust against occlusion.

References

- [1] Jimmy Lei Ba, Jamie Ryan Kiros, and Geoffrey E Hinton. Layer normalization. *arXiv preprint arXiv:1607.06450*, 2016. 4
- [2] Philipp Bergmann, Tim Meinhardt, and Laura Leal-Taixe. Tracking without bells and whistles. In *Proceedings of the IEEE/CVF International Conference on Computer Vision*, pages 941–951, 2019. 1

- [3] Keni Bernardin and Rainer Stiefelhagen. Evaluating multiple object tracking performance: the clear mot metrics. *EURASIP Journal on Image and Video Processing*, 2008:1–10, 2008. 6
- [4] Gary Bishop, Greg Welch, et al. An introduction to the kalman filter. *Proc of SIGGRAPH, Course*, 8(27599-23175):41, 2001. 2, 3, 7, 8, 9
- [5] Erik Bochinski, Volker Eiselein, and Thomas Sikora. High-speed tracking-by-detection without using image information. In *2017 14th IEEE International Conference on Advanced Video and Signal Based Surveillance (AVSS)*, pages 1–6. IEEE, 2017. 1, 3
- [6] Guillem Brasó and Laura Leal-Taixé. Learning a neural solver for multiple object tracking. In *Proceedings of the IEEE/CVF Conference on Computer Vision and Pattern Recognition*, pages 6247–6257, 2020. 1, 2, 4, 5
- [7] Zhaowei Cai, Quanfu Fan, Rogerio S Feris, and Nuno Vasconcelos. A unified multi-scale deep convolutional neural network for fast object detection. In *European Conference on Computer Vision*, pages 354–370. Springer, 2016. 6
- [8] Nicolas Carion, Francisco Massa, Gabriel Synnaeve, Nicolas Usunier, Alexander Kirillov, and Sergey Zagoruyko. End-to-end object detection with transformers. In *European Conference on Computer Vision*, pages 213–229. Springer, 2020. 5
- [9] Long Chen, Haizhou Ai, Zijie Zhuang, and Chong Shang. Real-time multiple people tracking with deeply learned candidate selection and person re-identification. In *2018 IEEE International Conference on Multimedia and Expo (ICME)*, pages 1–6. IEEE, 2018. 1
- [10] Luca Ciampi, Nicola Messina, Fabrizio Falchi, Claudio Genaro, and Giuseppe Amato. Virtual to real adaptation of pedestrian detectors. *Sensors*, 20(18):5250, 2020. 6
- [11] Peng Dai, Renliang Weng, Wongun Choi, Changshui Zhang, Zhangping He, and Wei Ding. Learning a proposal classifier for multiple object tracking. In *Proceedings of the IEEE/CVF Conference on Computer Vision and Pattern Recognition*, pages 2443–2452, 2021. 2
- [12] Patrick Dendorfer, Aljosa Osep, Anton Milan, Konrad Schindler, Daniel Cremers, Ian Reid, Stefan Roth, and Laura Leal-Taixé. Motchallenge: A benchmark for single-camera multiple target tracking. *International Journal of Computer Vision*, 129(4):845–881, 2021. 14
- [13] Patrick Dendorfer, Hamid Rezatofighi, Anton Milan, Javen Shi, Daniel Cremers, Ian Reid, Stefan Roth, Konrad Schindler, and Laura Leal-Taixé. Mot20: A benchmark for multi object tracking in crowded scenes. *arXiv preprint arXiv:2003.09003*, 2020. 6, 7, 13, 14
- [14] Piotr Dollár, Christian Wojek, Bernt Schiele, and Pietro Perona. Pedestrian detection: A benchmark. In *2009 IEEE Conference on Computer Vision and Pattern Recognition*, pages 304–311. IEEE, 2009. 6
- [15] Alexey Dosovitskiy, Philipp Fischer, Eddy Ilg, Philip Hausser, Caner Hazirbas, Vladimir Golkov, Patrick Van Der Smagt, Daniel Cremers, and Thomas Brox. FlowNet: Learning optical flow with convolutional networks. In *Proceedings of the IEEE International Conference on Computer Vision*, pages 2758–2766, 2015. 2
- [16] Andreas Ess, Bastian Leibe, Konrad Schindler, and Luc Van Gool. A mobile vision system for robust multi-person tracking. In *2008 IEEE Conference on Computer Vision and Pattern Recognition*, pages 1–8. IEEE, 2008. 6
- [17] Christoph Feichtenhofer, Axel Pinz, and Andrew Zisserman. Detect to track and track to detect. In *Proceedings of the IEEE International Conference on Computer Vision*, pages 3038–3046, 2017. 2
- [18] Justin Gilmer, Samuel S Schoenholz, Patrick F Riley, Oriol Vinyals, and George E Dahl. Neural message passing for quantum chemistry. In *International Conference on Machine Learning*, pages 1263–1272. PMLR, 2017. 2
- [19] Kaiming He, Xiangyu Zhang, Shaoqing Ren, and Jian Sun. Deep residual learning for image recognition. In *Proceedings of the IEEE Conference on Computer Vision and Pattern Recognition*, pages 770–778, 2016. 14
- [20] KJ Joseph, Salman Khan, Fahad Shahbaz Khan, and Vineeth N Balasubramanian. Towards open world object detection. In *Proceedings of the IEEE/CVF Conference on Computer Vision and Pattern Recognition*, pages 5830–5840, 2021. 7
- [21] Diederik P Kingma and Jimmy Ba. Adam: A method for stochastic optimization. *arXiv preprint arXiv:1412.6980*, 2014. 6
- [22] Thomas N Kipf and Max Welling. Semi-supervised classification with graph convolutional networks. *arXiv preprint arXiv:1609.02907*, 2016. 2
- [23] Harold W Kuhn. The hungarian method for the assignment problem. *Naval Research Logistics Quarterly*, 2(1-2):83–97, 1955. 3, 5
- [24] Hei Law and Jia Deng. Cornernet: Detecting objects as paired keypoints. In *Proceedings of the European Conference on Computer Vision (ECCV)*, pages 734–750, 2018. 5
- [25] Yuan Li, Chang Huang, and Ram Nevatia. Learning to associate: Hybridboosted multi-target tracker for crowded scene. In *2009 IEEE Conference on Computer Vision and Pattern Recognition*, pages 2953–2960. IEEE, 2009. 6
- [26] Chao Liang, Zhipeng Zhang, Yi Lu, Xue Zhou, Bing Li, Xiyong Ye, and Jianxiao Zou. Rethinking the competition between detection and reid in multi-object tracking. *arXiv preprint arXiv:2010.12138*, 2020. 2, 7
- [27] Chao Liang, Zhipeng Zhang, Xue Zhou, Bing Li, Yi Lu, and Weiming Hu. One more check: Making "fake background" be tracked again. *arXiv preprint arXiv:2104.09441*, 2021. 3, 7
- [28] Tsung-Yi Lin, Priya Goyal, Ross Girshick, Kaiming He, and Piotr Dollár. Focal loss for dense object detection. In *Proceedings of the IEEE International Conference on Computer Vision*, pages 2980–2988, 2017. 2, 5
- [29] Tsung-Yi Lin, Michael Maire, Serge Belongie, James Hays, Pietro Perona, Deva Ramanan, Piotr Dollár, and C Lawrence Zitnick. Microsoft coco: Common objects in context. In *European Conference on Computer Vision*, pages 740–755. Springer, 2014. 6
- [30] Zhichao Lu, Vivek Rathod, Ronny Votel, and Jonathan Huang. Retinatrack: Online single stage joint detection and tracking. In *Proceedings of the IEEE/CVF Conference*

- on *Computer Vision and Pattern Recognition*, pages 14668–14678, 2020. 1, 2
- [31] Anton Milan, Laura Leal-Taixé, Ian Reid, Stefan Roth, and Konrad Schindler. Mot16: A benchmark for multi-object tracking. *arXiv preprint arXiv:1603.00831*, 2016. 6, 7, 13
- [32] Christopher Morris, Martin Ritzert, Matthias Fey, William L Hamilton, Jan Eric Lenssen, Gaurav Rattan, and Martin Grohe. Weisfeiler and leman go neural: Higher-order graph neural networks. In *Proceedings of the AAAI Conference on Artificial Intelligence*, volume 33, pages 4602–4609, 2019. 2
- [33] Alejandro Newell, Kaiyu Yang, and Jia Deng. Stacked hourglass networks for human pose estimation. In *European Conference on Computer Vision*, pages 483–499. Springer, 2016. 14
- [34] Kenta Oono and Taiji Suzuki. Graph neural networks exponentially lose expressive power for node classification. *arXiv preprint arXiv:1905.10947*, 2019. 5
- [35] Jiangmiao Pang, Linlu Qiu, Xia Li, Haofeng Chen, Qi Li, Trevor Darrell, and Fisher Yu. Quasi-dense similarity learning for multiple object tracking. In *IEEE/CVF Conference on Computer Vision and Pattern Recognition*, June 2021. 6, 7
- [36] Jinlong Peng, Yueyang Gu, Yabiao Wang, Chengjie Wang, Jilin Li, and Feiyue Huang. Dense scene multiple object tracking with box-plane matching. In *Proceedings of the 28th ACM International Conference on Multimedia*, pages 4615–4619, 2020. 1
- [37] Jinlong Peng, Changan Wang, Fangbin Wan, Yang Wu, Yabiao Wang, Ying Tai, Chengjie Wang, Jilin Li, Feiyue Huang, and Yanwei Fu. Chained-tracker: Chaining paired attentive regression results for end-to-end joint multiple-object detection and tracking. In *European Conference on Computer Vision*, pages 145–161. Springer, 2020. 1, 2
- [38] Joseph Redmon and Ali Farhadi. Yolov3: An incremental improvement. *arXiv preprint arXiv:1804.02767*, 2018. 2
- [39] Shaoqing Ren, Kaiming He, Ross Girshick, and Jian Sun. Faster r-cnn: Towards real-time object detection with region proposal networks. *Advances in Neural Information Processing Systems*, 28, 2015. 2, 6
- [40] Ergys Ristani, Francesco Solera, Roger Zou, Rita Cucchiara, and Carlo Tomasi. Performance measures and a data set for multi-target, multi-camera tracking. In *European Conference on Computer Vision*, pages 17–35. Springer, 2016. 6
- [41] Shuai Shao, Zijian Zhao, Boxun Li, Tete Xiao, Gang Yu, Xiangyu Zhang, and Jian Sun. Crowdhuman: A benchmark for detecting human in a crowd. *arXiv preprint arXiv:1805.00123*, 2018. 6, 13, 14
- [42] Bing Shuai, Andrew Berneshawi, Manchen Wang, Chunhui Liu, Davide Modolo, Xinyu Li, and Joseph Tighe. Application of multi-object tracking with siamese track-rcnn to the human in events dataset. In *Proceedings of the 28th ACM International Conference on Multimedia*, pages 4625–4629, 2020. 1, 2
- [43] Peize Sun, Yi Jiang, Rufeng Zhang, Enze Xie, Jinkun Cao, Xinting Hu, Tao Kong, Zehuan Yuan, Changhu Wang, and Ping Luo. Transtrack: Multiple-object tracking with transformer. *arXiv preprint arXiv:2012.15460*, 2020. 2, 7
- [44] Gaoang Wang, Yizhou Wang, Haotian Zhang, Renshu Gu, and Jenq-Neng Hwang. Exploit the connectivity: Multi-object tracking with trackletnet. In *Proceedings of the 27th ACM International Conference on Multimedia*, pages 482–490, 2019. 1, 2
- [45] Qiang Wang, Yun Zheng, Pan Pan, and Yinghui Xu. Multiple object tracking with correlation learning. In *Proceedings of the IEEE/CVF Conference on Computer Vision and Pattern Recognition*, pages 3876–3886, 2021. 2, 3, 5, 6, 7, 8, 13, 14
- [46] Yongxin Wang, Kris Kitani, and Xinshuo Weng. Joint object detection and multi-object tracking with graph neural networks. In *2021 IEEE International Conference on Robotics and Automation (ICRA)*, pages 13708–13715. IEEE, 2021. 2, 3, 6, 7, 8, 14
- [47] Zhongdao Wang, Liang Zheng, Yixuan Liu, Yali Li, and Shengjin Wang. Towards real-time multi-object tracking. In *European Conference on Computer Vision*, pages 107–122. Springer, 2020. 1, 2, 3, 5, 6
- [48] Xinshuo Weng, Yongxin Wang, Yunze Man, and Kris M Kitani. Gnn3dmot: Graph neural network for 3d multi-object tracking with 2d-3d multi-feature learning. In *Proceedings of the IEEE/CVF Conference on Computer Vision and Pattern Recognition*, pages 6499–6508, 2020. 4
- [49] Nicolai Wojke, Alex Bewley, and Dietrich Paulus. Simple online and realtime tracking with a deep association metric. In *2017 IEEE International Conference on Image Processing (ICIP)*, pages 3645–3649. IEEE, 2017. 1
- [50] Jialian Wu, Jiale Cao, Liangchen Song, Yu Wang, Ming Yang, and Junsong Yuan. Track to detect and segment: An online multi-object tracker. In *Proceedings of the IEEE/CVF Conference on Computer Vision and Pattern Recognition*, pages 12352–12361, 2021. 2, 3, 6, 7
- [51] Tong Xiao, Shuang Li, Bochao Wang, Liang Lin, and Xiaogang Wang. Joint detection and identification feature learning for person search. In *Proceedings of the IEEE Conference on Computer Vision and Pattern Recognition*, pages 3415–3424, 2017. 6
- [52] Jiarui Xu, Yue Cao, Zheng Zhang, and Han Hu. Spatial-temporal relation networks for multi-object tracking. In *Proceedings of the IEEE/CVF International Conference on Computer Vision*, pages 3988–3998, 2019. 1, 2, 4
- [53] Yihong Xu, Yutong Ban, Guillaume Delorme, Chuang Gan, Daniela Rus, and Xavier Alameda-Pineda. Transcenter: Transformers with dense queries for multiple-object tracking. *arXiv preprint arXiv:2103.15145*, 2021. 7
- [54] En Yu, Zhuoling Li, Shoudong Han, and Hongwei Wang. Relationtrack: Relation-aware multiple object tracking with decoupled representation. *arXiv preprint arXiv:2105.04322*, 2021. 2, 6, 7
- [55] Fisher Yu, Dequan Wang, Evan Shelhamer, and Trevor Darrell. Deep layer aggregation. In *Proceedings of the IEEE Conference on Computer Vision and Pattern Recognition*, pages 2403–2412, 2018. 3, 14
- [56] Hongyang Yu, Guorong Li, Weigang Zhang, Hongxun Yao, and Qingming Huang. Self-balance motion and appearance model for multi-object tracking in uav. In *Proceedings of the ACM Multimedia Asia*, pages 1–6. 2019. 1

- [57] Shanshan Zhang, Rodrigo Benenson, and Bernt Schiele. Citypersons: A diverse dataset for pedestrian detection. In *Proceedings of the IEEE Conference on Computer Vision and Pattern Recognition*, pages 3213–3221, 2017. 6
- [58] Wei Zhang, Lingxiao He, Peng Chen, Xingyu Liao, Wu Liu, Qi Li, and Zhenan Sun. Boosting end-to-end multi-object tracking and person search via knowledge distillation. In *Proceedings of the 29th ACM International Conference on Multimedia*, pages 1192–1201, 2021. 6, 7
- [59] Yifu Zhang, Peize Sun, Yi Jiang, Dongdong Yu, Zehuan Yuan, Ping Luo, Wenyu Liu, and Xinggang Wang. Byte-track: Multi-object tracking by associating every detection box. *arXiv preprint arXiv:2110.06864*, 2021. 3, 8
- [60] Yifu Zhang, Chunyu Wang, Xinggang Wang, Wenjun Zeng, and Wenyu Liu. Fairmot: On the fairness of detection and re-identification in multiple object tracking. *International Journal of Computer Vision*, 129(11):3069–3087, 2021. 1, 2, 3, 5, 6, 7, 8, 14
- [61] Linyu Zheng, Ming Tang, Yingying Chen, Guibo Zhu, Jin-qiao Wang, and Hanqing Lu. Improving multiple object tracking with single object tracking. In *Proceedings of the IEEE/CVF Conference on Computer Vision and Pattern Recognition*, pages 2453–2462, 2021. 7, 8, 14
- [62] Liang Zheng, Hengheng Zhang, Shaoyan Sun, Manmohan Chandraker, Yi Yang, and Qi Tian. Person re-identification in the wild. In *Proceedings of the IEEE Conference on Computer Vision and Pattern Recognition*, pages 1367–1376, 2017. 6
- [63] Xingyi Zhou, Vladlen Koltun, and Philipp Krähenbühl. Tracking objects as points. In *European Conference on Computer Vision*, pages 474–490. Springer, 2020. 1, 2, 6, 7
- [64] Xingyi Zhou, Dequan Wang, and Philipp Krähenbühl. Objects as points. *arXiv preprint arXiv:1904.07850*, 2019. 2, 3, 5, 6, 8, 14
- [65] Ji Zhu, Hua Yang, Nian Liu, Minyoung Kim, Wenjun Zhang, and Ming-Hsuan Yang. Online multi-object tracking with dual matching attention networks. In *Proceedings of the European Conference on Computer Vision (ECCV)*, pages 366–382, 2018. 1
- [66] Xizhou Zhu, Weijie Su, Lewei Lu, Bin Li, Xiaogang Wang, and Jifeng Dai. Deformable detr: Deformable transformers for end-to-end object detection. In *International Conference on Learning Representations*, 2021. 2, 7

A. Appendix

In this appendix, we provide additional implementation details, experiment results, analysis, and visualization results that were not included in the main paper due to space limitations. The organization is as follows:

1. Section A.1 describes the details of implementation.
2. Section A.2 compares using low thresholding and top- K sampling of detections for building a graph in SGT.
3. Section A.3 shows the ratio of recovered detections for each sequence in MOT17/20. In the sequences with the highest recovery ratio, SGT achieves the largest improvement of MOTA compared with other sequences in MOT17/20.
4. Section A.4 reports additional ablation experiments.
5. Section A.5 presents additional visualization results of detection recovery cases in MOT20 test dataset.

A.1. Implementation Details

We use different training epochs and loss weight terms for the ablation experiments in the main paper which do not use CrowdHuman dataset [41] as extra training dataset but only use half of MOT17 training dataset [31]. SGT is trained for 30 epochs and learning rate is dropped from $2e^{-4}$ to $2e^{-5}$ at 20 epoch. The same detection loss weights are adopted, but we use w_{edge} as 1, instead of 0.1. When SGT is trained with $K = 500$, w_{node} decreases from 10 to 5 due to larger scale of loss. All these values are chosen empirically.

A.2. Low Threshold vs Top-K

SGT can achieve detection recovery by including detections which score is below the detection threshold in the association step. In the main paper, our experiments were based on top- K detections with a large K value, such as 100 or 300. Introducing an extra low detection threshold (τ_{low}), instead of top- K , is another option to include low-scored detections, but τ_{low} is a sensitive parameter to be carefully tuned for the datasets. In the main paper, we already demonstrated the robustness of top- K method by showing the consistent performance with different K values ranging from 50 to 500.

In this appendix, we conduct the experiment that SGT is trained and evaluated with different K and τ_{low} values. Table 9 shows that the performance of using K of 300 and 50 for inference is consistent even when SGT is trained with τ_{low} , instead of top- K . In contrast, when SGT adopts τ_{low} for inference, the performance decreases with increasing τ_{low} . Although the performance is consistent when SGT is trained with $\tau_{low} = 0.1$, finding such an optimal parameter increases the complexity of training. Also, in the training phase, using higher τ_{low} of 0.1 rather than 0.01 leads SGT to output consistent performance; however, in the in-

Table 9. Ablation study of low threshold and top- K for choosing detection candidates as nodes in a graph. SGT is trained on the first half of MOT17 train dataset and CrowdHuman dataset, and evaluated on the MOT17 validation dataset with different low threshold and K values.

train	inference	MOTA \uparrow	IDF1 \uparrow	FP \downarrow	FN \downarrow	IDS \downarrow
$K = 300$	$K = 300$	73.7	73.9	2616	11040	556
$K = 300$	$K = 50$	73.7	74.3	2522	11145	529
$K = 300$	$\tau_{low} = 0.1$	72.5	71.0	2333	11410	1118
$K = 300$	$\tau_{low} = 0.3$	71.9	69.4	2248	11598	1338
$K = 100$	$K = 300$	74.1	76.2	2543	10967	496
$K = 100$	$K = 50$	74.1	75.4	2496	11013	511
$K = 100$	$\tau_{low} = 0.1$	73.5	73.2	2400	11144	770
$K = 100$	$\tau_{low} = 0.3$	72.7	70.6	2345	11305	1101
$\tau_{low} = 0.01$	$K = 300$	74.3	74.8	2550	10785	572
$\tau_{low} = 0.01$	$K = 50$	74.1	75.7	2477	10922	583
$\tau_{low} = 0.01$	$\tau_{low} = 0.1$	72.8	71.9	2429	11045	1247
$\tau_{low} = 0.01$	$\tau_{low} = 0.3$	71.4	70.3	2322	11346	1799
$\tau_{low} = 0.1$	$K = 300$	73.8	75.2	2859	10765	522
$\tau_{low} = 0.1$	$K = 50$	73.9	75.3	2802	10747	542
$\tau_{low} = 0.1$	$\tau_{low} = 0.1$	73.8	74.5	2843	10795	529
$\tau_{low} = 0.1$	$\tau_{low} = 0.3$	73.6	74.8	2883	10806	585

Table 10. Ratio of recovered detections over all detections in each sequence of MOT17/20 test datasets.

Sequence	$\frac{\#recovery}{\#dets}$ (%)
MOT17 [31]	
MOT17-01	11.9
MOT17-03	1.7
MOT17-06	6.7
MOT17-07	9.9
MOT17-08	14.3
MOT17-12	10.3
MOT17-14	12.5
MOT20 [13]	
MOT20-04	3.7
MOT20-06	29.0
MOT20-07	4.9
MOT20-08	35.2

ference phase, using lower τ_{low} of 0.1 instead of 0.3 increases MOTA. In other words, the optimal value for τ_{low} is different for the training and inference phases. Due to this issue of τ_{low} , we developed SGT based on top- K .

A.3. Ratio of Recovered Detections

We further support the effectiveness of detection recovery in SGT based on the ratio of recovered detections over detections for each sequence of MOT17 [31] and MOT20 [13]. As shown in Table 10, SGT outputs the highest ratio of recovered detections in MOT17-08 and MOT20-08 sequences. In these two sequences, SGT surpasses other methods in terms of MOTA with the highest gap as shown in Table 11. Specifically, SGT achieves slightly lower MOTA than CorrTracker [45] in the average of MOT17 sequences;



Figure 6. Detection recovery cases in MOT20 test dataset [13]. We show the annotation of each prediction box in the format of “{id}-{detection score}”. The detection threshold value is 0.5 so the objects which score below 0.5 are recovered detections.

Table 11. Evaluation results of MOT17/20 sequences collected from MOTChallenge leaderboard. MT and ML are computed by the number of ground-truth tracklets from [12, 13].

Method	MOTA↑	IDF1↑	MT↑	ML↓	FP↓	FN↓	IDS↓
MOT17-06 (6.7% recovery)							
SGT (ours)	65.4	63.6	48.2	12.2	941	2918	220
FairMOT [60]	64.1	65.9	40.1	18.5	526	3533	176
GSDT [46]	63.0	62.0	40.1	21.2	681	3500	180
CorrTracker [45]	66.2	68.2	41.0	17.1	465	3346	171
MOT17-08 (14.3% recovery)							
SGT (ours)	52.6	43.7	31.6	14.5	1071	8560	374
FairMOT [60]	42.2	42.0	22.4	28.9	776	11191	237
GSDT [46]	44.0	40.5	26.3	22.4	991	10523	323
CorrTracker [45]	49.9	46.7	25.0	17.1	1137	9201	250
MOT20-07 (4.9% recovery)							
SGT (ours)	77.8	71.1	76.6	2.7	2283	4775	281
FairMOT [60]	75.6	70.0	76.6	0.9	2988	4770	333
GSDT [46]	75.0	68.1	64.0	1.8	1870	6115	282
SOTMOT [61]	72.6	71.2	76.6	2.7	3675	5066	317
MOT20-08 (35.2% recovery)							
SGT (ours)	54.1	53.3	26.7	25.7	2451	32598	508
FairMOT [60]	27.0	49.5	41.9	14.7	32104	23447	981
GSDT [46]	39.4	48.9	22.5	32.5	9916	36420	608
SOTMOT [61]	43.1	55.1	35.6	19.9	16025	27216	863

however, in MOT17-08 sequence which consists of the highest recovery ratio, SGT shows 2.7% higher MOTA than CorrTracker [45]. Also, in MOT20-08 sequence, SGT surpasses SOTMOT [61] in MOTA by 11.0% which gap is much larger than the gap in MOT20-07.

A.4. Additional Ablation Studies

Here, we provide the results of SGT and FairMOT [60] using different backbones [19, 33, 55]. For the hourglass backbone network [33], we use an image size of $(H, W) = (640, 1152)$, instead of $(608, 1088)$ since only a multiple of

Table 12. Ablation study on different backbones. Original model is based on the dla34 backbone network [55]. Here, we compare with FairMOT [60] based on the resnet18/101 [19] and hourglass104 [33] networks which are modified with additional upsampling layers as in CenterNet [64]. The models are trained with an extra CrowdHuman [41] dataset.

Model	Backbone	MOTA↑	IDF1↑	MT↑	ML↓	FP↓	FN↓	IDS↓
FairMOT [60]	resdcn18	66.1	69.9	40.1	20.4	2036	16029	265
SGT (ours)	resdcn18	68.1	69.6	47.8	15.0	2777	13719	738
FairMOT [60]	resdcn101	70.2	72.2	47.8	14.5	2545	13178	364
SGT (ours)	resdcn101	70.5	70.5	53.7	12.4	3201	11853	912
FairMOT [60]	dladcn34	72.2	74.7	47.8	18.0	2660	12025	336
SGT (ours)	dladcn34	74.1	76.1	53.1	13.6	2514	10973	491
FairMOT [60]	hg104	74.4	77.1	54.0	12.1	2636	10844	344
SGT (ours)	hg104	74.6	75.4	54.9	11.5	2894	10370	470

128 is allowed. According to Table 12, SGT achieves lower FN and ML, and higher MT and MOTA than FairMOT [60] across all backbone networks. These indicate that SGT has less number of missed detections and more stable tracklets than FairMOT [60] which are the effects of detection recovery. Thus, our proposed detection recovery with SGT works well regardless of the backbone networks to output the better trade-off between FP and FN.

A.5. Additional Visualization Results

Figure 6 shows the examples of detection recovery in MOT20 test dataset. In the first row, people labeled by the blue and brown bounding boxes are occluded each other. From frame #34 to #37, their detection scores are below the detection threshold and they were missed detections originally; however, SGT successfully recovers them by including low-scored detections in the association step, Figure 6

also shows the detection recovery case of people labeled by the green and orange bounding boxes in the second row.